Measurement xxx (xxxx) xxx

Contents lists available at ScienceDirect

Measurement

journal homepage: www.elsevier.com/locate/measurement

A portable low-cost reflectometric setup for moisture measurement in cultural heritage masonry unit

Livio D'Alvia [a,*], Erika Pittella [b], Emanuele Rizzuto [a], Emanuele Piuzzi [c], Zaccaria Del Prete [a]

[a] Department of Mechanical and Aerospace Engineering, Sapienza University of Rome, Rome, Italy
[b] Department of Legal and Economic Sciences, Pegaso University, Naples, Italy
[c] Department of Information Engineering, Electronics and Telecommunications, Sapienza University of Rome, Rome, Italy

ARTICLE INFO

Keywords:
Moisture measurements
Microwave reflectometry
Load-cell
Calibration curve
Non-invasive measurement
Sensing device
miniVNA-TINY
Instrumentation design
Archaeometry
Cultural heritage

ABSTRACT

A low-cost and portable reflectometric system was described to correlate the water content inside building material with the resonance frequency of a planar probe. An inexpensive planar patch resonator was realized, and a high sensitivity load cell was developed to investigate the external force effect on the resonance frequency shift. Regarding the material under test, four stones commonly employed in Italy Cultural Heritage buildings were used: *Pietra Gentile, Leccese, Carparo,* and *Tuff.* Measurements were carried out at different water content values and were performed using a portable vector network analyzer. Two different trials were carried out ten times for each moisture level: with an unknown handheld force exerted on the probe and using the load cell to ensure a repeatable force. Results showed that a repeatable applied force guaranteed more reproducible measurements. The achieved humidity/frequency calibration curves can be used, in practice, for non-invasive on-site water content monitoring of historic structures.

1. Introduction

In many engineering processes such as pharmaceutical, chemical, food, energy, the measurement of the physical characteristics and structural composition of bulk, granular, or composite materials plays a central role [1–3]. For composites, the measurement of the thickness of the dielectric materials, the distribution of different compounds, or the presence and dimension of discontinuities is critical in the quality control processes [4]. Another essential element to consider is the presence of undesired compounds (water, residual solvent, salt) that could compromise quality assessment results [5,6]. Monitoring Cultural Heritage artifacts is undoubtedly a field of measurement as appealing as challenging, given the considerable diversification of materials under investigation and the physicochemical/mechanical interactions with the surrounding environment.

Although the phenomena involved in the deterioration of ancient structures are multiple, the hydrothermal variation represents the most significant cause of material decay in ancient buildings. Excessively high moisture levels may have dramatic consequences on the preservation of heritages: water, alone or combined with pollutant or temperature, could jeopardize the completeness, intelligibility, and integrity of the: masterpiece like manuscripts, petroglyphs, frescos, and paintings; or structural materials like wood masonry units, paper [7,8]. This work pays attention to masonry materials: due to their permeability, absorption or water imbibition may promote decay processes of different nature as, for example, biological activity, superficial layer erosion, coloring, or internal cohesion [9,10].

Over the last decade, the scientific community's interest in monitoring historic buildings, dedicated technologies, and non-invasive methodologies has considerably increased. Indeed a wide range of measurement instrumentations and methods are applied to evaluate water content [11,12]; in particular electromagnetic methods that associate the moisture level to permittivity measurements have become appealing solutions. Traditional techniques and instruments [13,14] are briefly presented and summarized below.

Nuclear magnetic resonance (NMR) is a non-destructive technique based on the interaction between a magnetic field pulsed at the radio-frequency and hydrogen atoms giving direct information about the relative abundance of water in solid material, showing water distribution inside materials with a false-color image. This method presents both contact and contactless probes.[15–18].

Near-infrared spectrometry (NIRS) is a contactless, fast and non-

* Corresponding author at: Dept. of Mechanical and Aerospace Engineering, Sapienza Università di Roma, Via Eudossiana, 18, Rome 00184, Italy.
E-mail addresses: livio.dalvia@uniroma1.it (L. D'Alvia), erika.pittella@unipegaso.it (E. Pittella), emanuele.rizzuto@uniroma1.it (E. Rizzuto), emanuele.piuzzi@uniroma1.it (E. Piuzzi), zaccaria.delprete@uniroma1.it (Z. Del Prete).

https://doi.org/10.1016/j.measurement.2021.110438
Received 25 January 2021; Received in revised form 27 October 2021; Accepted 4 November 2021
Available online 11 November 2021

Table 1
Resonator features.

Parameters	Values
$L = W$	48 mm
t	3.175 mm
ε_{sub}	2.32
f_r	1.95 GHz

destructive technique that provides multicomponent analysis and can be employed for the real-time measurement of moisture, either in the laboratory and on-site [19].

Thermography is based on thermal images realized with a camera sensitive to IR spectral range. Even if the camera measures the surface temperature gradient and variations directly, it is possible to detect the consequences of moisture content (rising damp, air leakage, molding) [20–22].

Ultrasound is a contact method based on the reflection or transmission of ultrasonic signals to detect travel time through a material under test. It depends on the material's physical and mechanical properties and the moisture content that increases the speed in materials like cement, mortar, concrete, or stone [23,24].

Resistive/Conductive instruments are based on contact probes that measure the current intensity flowing through two electrodes in contact with the surface layer or through two pins inserted in the material at a depth between 1 and 100 mm [25–27]. In masonry and stone, the impedance decreases with an increase of moisture content and in the presence of salt. This is a comparative method, with arbitrary units as output, and often returns a comparison with gravimetric results to obtain a percent scale. If temperature, density, and the kind of materials represent significant disadvantages of these instruments, the principal advantages regard the non-destructivity (or micro-destructivity if needles are inserted) and the possibility of achieving real-time measurement.

Electrical Capacity (or dielectric) instruments are based on contact probes that measure capacitance variation due to water presence between the electrodes [28]. The physical principle regulating this kind of instrument regards the variation of the material dielectric response, increasing proportionally with moisture content: dry materials often used in cultural heritage buildings have a low relative permittivity $2 < \varepsilon_r < 8$ whereas water has $\varepsilon_r = 80$. For brickworks, this method is independent of soluble salt presence; however, it depends on internal discontinuities or cavities and variation in density. Moreover, the output is not linear, and the accuracy decreases with high moisture content.

Microwave methods are based on a planar resonator assembly that radiates into the material at radiofrequency. When the microwave beam interacts with water molecules, it loses energy, decreases power intensity, and shows a phase shift [29]. This method is influenced by material thickness and density; if the beam is not wholly extinguished within the material, it has a back reflection that alters the reading when it reaches the ending surface. It finds application in walls and timber structures [30,31].

A particular application of microwave devices is the contact and not-invasive *Evanescent-field dielectrometry (EFD)* method that operates in the range of 1–3 GHz. As discussed for capacitive devices, the method works to differentiate the signal caused by water from the signal due to the bulk material, which has a lower relative permittivity. The signal is composed of a real and an imaginary part of permittivity, where the real one is measured as resonance frequency shift and depends on moisture content. The probe is based on a microstrip resonant probe coupled with an open-coaxial [32–34].

Another microwave application is the *Time-domain Reflectometry (TDR),* another contact and not-invasive (or micro-destructive if needle probes are inserted) method that measures the travel time between transmission and response of a radio signal [35,36] to determine the relative permittivity of the material: a slight variation of water produces a significant outcome on the relative permittivity of material under test.

In recent years, reflectometry played a leading role in water content measurements and building material diagnosis, thanks to developing low-cost and tailored probes with adequate measurement accuracy [37]. Probes are commonly based on coaxial or multi rod probes [36,38], while nowadays, conductive strips have been explored as possible planar probes for reflectometric application, resulting in a high-performing method for applications in which noninvasive measurements are required. For example, in Cultural Heritage, they are often used to monitor building materials, wall-painting, architectonic surfaces, or structures [39]. Recent studies in the field of Cultural Heritage [40,41] proposed a square patch resonator, connected to a bench vector network analyzer (VNA), as planar reflectometric probe. As a result, the patch resonance frequency changes are directly related to the corresponding moisture content θ, thus going beyond the traditional method. The moisture percentage level is assessed by determining the apparent dielectric permittivity ε. However, Piuzzi et al. [41,42] have tested a planar tailored microstrip resonator that embedded a soft-conductive layer (conductive silicon) to increase the adhesion to the material under test and consequently the measurement repeatability and reduce hazards on the material in a future application.

Within this context, in this work, a portable, easy-to-use, and non-invasive microwave reflectometry-based measurement setup is proposed, whose probe integrates a patch resonator and a customized load cell. The proposed solution is based on a square patch resonator, a portable vector network analyzer (miniVNA-TINY), and a custom-built load cell comprising the conditioning signal module.

The proposed measurement system, described in depth in Section 2, reckons two stages. First, we evaluated the correlation between the resonance frequency and the applied force for dried stones, identifying a limiting point beyond which a frequency shift did not occur. Subsequently, we correlated the resonance frequency with nine different moisture content levels θ_v for four types of stone: *Leccese, Carparo,* and *Gentile stones*, widely employed in Apulian cultural heritage structures; and *Tuff,* widely used since ancient roman times to the present day in Latium and Campania buildings. Each test was repeated ten times in two distinct conditions: the standard way, without controlling the applied force, and the load cell to ensure the desired applied force. The results are shown and discussed in Section 3, while significant achievements and future works are outlined in Section 4.

2. Experimental setup

2.1. Measurement probe

We used a square patch resonator parametrized to obtain a resonance frequency f_r equal to 1.95 GHz and covered by a soft electrically conductive silicon layer to improve the adherence between stone surface and resonator [40]. This frequency was chosen as a compromise between the probe size and the external reader frequency range, as discussed below. Table 1 shows the most significant parameters used as the patch size – length L, width W, thickness t of the patch substrate – and the laminate dielectric constant ε_{sub}.

In general, for a microstrip patch resonator, the resonance frequency f_r depends on the effective length L_{eff} and the effective relative permittivity ε_{eff} of the resonator [43]. Either parameter is strictly correlated to the resonator geometry, to the relative permittivity of the patch dielectric substrate ε_{sub} and the upper medium in direct contact with the patch ε_m. As a result, the resonance frequency may be directly correlated to the upper medium dielectric characteristics. Therefore, a practical way to evaluate f_r is to associate the resonance frequency with the frequency corresponding at the minimum of the reflection coefficient magnitude $|S_{11}(f)|$ that, in turn, is intrinsically associated with ε_m. Starting from these considerations, it is also possible to evaluate the variation of f_r due to material inhomogeneities. The thickness h of the material sample placed over the resonator was supposed sufficiently

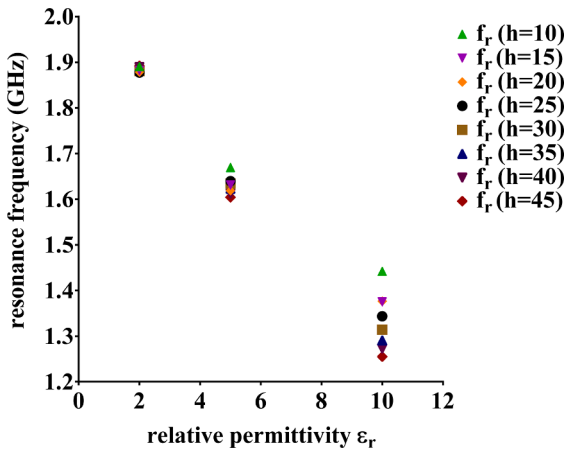

Fig. 1. Numerical evaluation of the resonance frequency as a function of material permittivity and thickness h in mm.

thick to ensure that the electromagnetic field was entirely confined into the medium. Fig. 1 shows a numerical evaluation of the patch resonance frequency as a function of the sample permittivity ε_m and thickness h in mm. The figure highlights that the patch, up to material dielectric permittivity $\varepsilon_m = 5$, requires a material thickness of 15 mm, while increasing the ε_m a greater thickness is required.

The probe was then connected to a MiniVNA-TINY, a low-cost (≈ 430 €), compact (66 mm × 66 mm × 28 mm), and portable (70 g) device antenna analyzer as shown in Fig. 2. The device has a frequency range from 0.001 GHz to 3 GHz. As VNA, the device allows measuring: signal wave ratio (SWR), antenna impedance (50 Ω to 1 kΩ), and scattering parameters. Moreover, a USB interface allows the power supply and serial communication with a PC/SmartPhone, which supports the javascript opensource software VNA/J [44]. Finally, the MINI-WNA was calibrated through the calibration kit provided by the WIMO manufacturing company based on SMA open, short and 50 Ω termination.

2.2. Force measurement device

To ensure a proper force applied on the square patch, we devised a bending pancake load-cell, according to the following characteristics: sufficiently small to be contained within the resonator surface; able to read low-intensity loads up to a maximum of 55 N; low cross-sensitivity for tensile/compression deformations generated by non-axial loads.

The so-realized load cell, parameterized with a diameter equal to 40 mm, is based on a cross between two beams fixed at both ends with a center load, which guarantees low cross-sensitivity by non-axial load (tensile/compression deformations) [45], and an axial sensitivity of 26.25 mV/N in the range 0 N to 55 N. The load cell was then connected to a breakout board that embeds an HX711 Analog-to-Digital Converter (ADC) [46]. The main features of this device are the on-chip power supply regulator, the internal selectable gain, a low noise, and an easy-to-program digital interface. The ADC digital output was connected to an Arduino Uno board, programmed to blink when the chosen force was achieved with an accuracy of 1 N, as reported in Fig. 3.

2.3. Material under test

The measurements were conducted on: (i) Tuff, widely used since ancient Rome times to the present day in Latium and Campania buildings; and (ii) three facies of Leccese stone (*Leccese, Gentile,* and *Carparo*), widely used in Apulian cultural heritage structures. Fig. 4 reports brick samples.

Tuff stone is a pyroclastic rock formed by aggregating ash and lapilli with dimensions between 2 mm and 30 mm, emitted during a volcanic eruption. This stone was regularly used in architecture, construction, and ornamental since Campania Magna Grecia and ancient Rome, thanks to its relative softness and high availability having the territories of the two regions a volcanic lithogenesis [47].

Improperly named "white tuff" due to the similar appearance, Leccese stones are organogenic sedimentary rocks. The three proposed facies represent three different lithological marlstone varieties distinguishable by their granulometry. More specifically:

- *Gentile* is the lithological variety characterized by a more homogeneous fine grain [48];
- *Leccese* is a marl organogenic calcarenite homogeneous grain with a higher superficial roughness than Gentile [49];
- *Carparo* is limestone with an evident roughness related to the marine environment sedimentation process, which involves shell cementation [50].

These stones are traditional building material, used mainly in the Salento area, as much in public and private buildings as an ornamental stone thanks to good workability properties, but, unfortunately, they

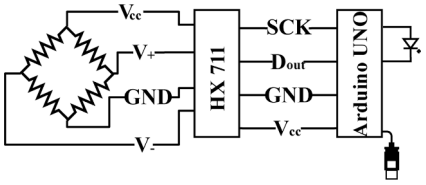

Fig. 3. Proposed load cell system schematic.

(a) (b)

Fig. 2. Proposed system. (**a**) Patch resonator with the electrically conductive silicon layer; (**b**) probe and miniVNA-Tiny.

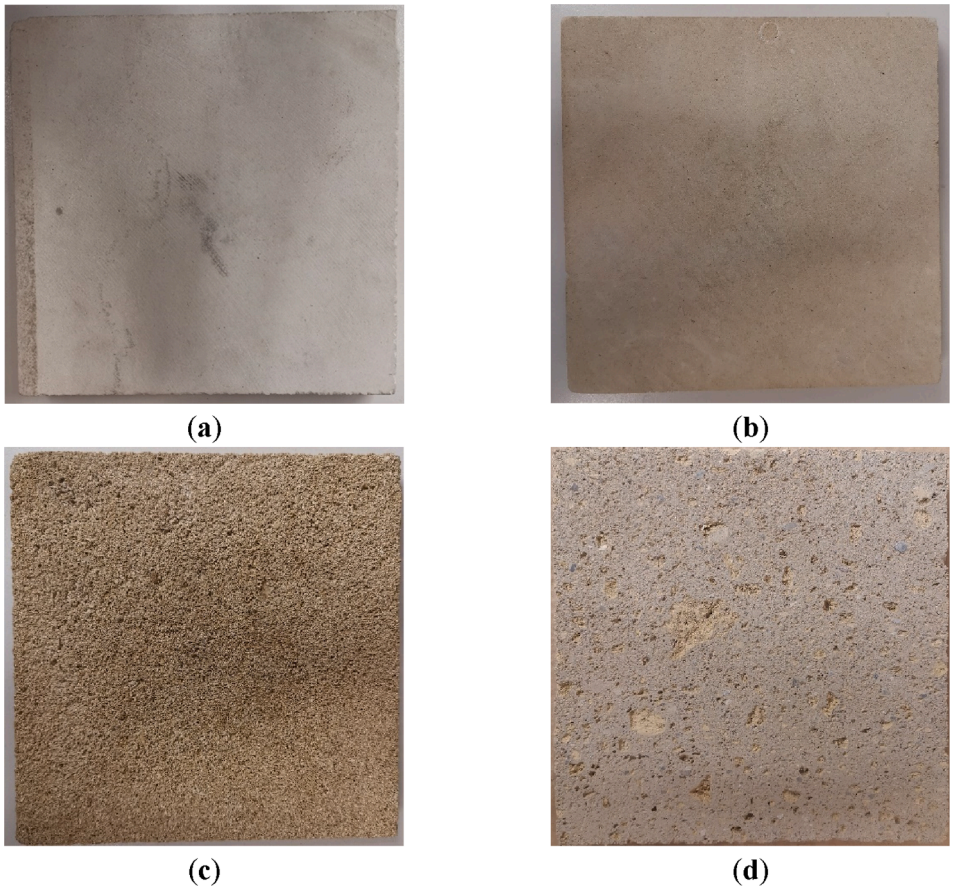

Fig. 4. Kind of bricks used for the tests. (**a**) Gentile Stone; (**b**) Leccese Stone; (**c**) Carparo; (d) Yellow Tuff. (For interpretation of the references to color in this figure legend, the reader is referred to the web version of this article.)

Table 2
Brick features

Stone name	Volume (cm^3)	Thickness (cm)	Dry weight (kg)
Leccese	788	2.0	1.981
Gentile	906	2.3	1.329
Carparo	823	2.1	1.255
Roman Tuff	861	2.1	1.068

tend to absorb and retain water, and therefore to degrade.

For the purposes of this work, the proposed materials were cut and leveled as much as possible, realizing four squared bricks with a surface of about 400 cm^2 and a thickness of about 2 cm, whose characteristics are shown in Table 2. Of note, this thickness allows a wholly confined electromagnetic field.

To confirm that the chosen depth allows a wholly confined electromagnetic field, we performed a series of preliminary tests placing an aluminum foil with a thickness of 3 cm and a surface of 0,08 m^2, behind each dry stone and measured the $|S_{11}(f)|$, to evaluate if there were any variations. For each condition, ten repetitions were done, and a test for statistical significance was carried out.

2.4. Measurement procedures

As stated above, in this paper, we explored the possibility of a non-invasive water content measurement through the evaluation of the resonance frequency *fr* shift. The dielectric properties of a material were linked with the variations in reflection scattering parameters $|S_{11}(f)|$ occurring when the radiating probe was positioned on the material surface. More precisely, as can be inferred from theory, the changes in the resonance frequency f_r of the probe can be related to the water content in the material under test [43].

As a preliminary test, we evaluated the capability of the sensor to discriminate four known plastic materials with a permittivity $1.6 < \varepsilon_r < 2.8$ in the range 1.72–2.60 GHz, more precisely:

- Low-Density Polyvinyl Chloride (LD-PVC) with $\varepsilon_r = 1.62$.
- Polytetrafluoroethylene (PTFE) with $\varepsilon_r = 2.06$.
- PolyMethyl Methacrylate (PMMA) with $\varepsilon_r = 2.60$.
- Polycarbonate (PC) with $\varepsilon_r = 2.80$.

The dielectric constants obtained by measurements were compared with the values provided by literature [51] using the graduation curve presented in [52].

The measurement procedure was organized in two steps and involved the four stones proposed. First, we investigated the asymptotic limit on the curve force-resonance frequency, assuming a maximum of 55 N as external force applicable on cultural heritage surfaces [53]. In the second, we investigated the $\theta_v - f_r$ relationships obtained through the miniVNA by varying the water content.

In the first step, we have applied twenty different force levels with a step of 1 N in the range 0 N to 10 N and 5 N in the range 10 N to 55 N studying the correlation between the patch response and the externally applied load. For each stone and each applied force value, we performed 10 repeated measurements to evaluate how the repeatability was affected by external load changes. In the first step, we took advantage of a custom built system, based on a linear actuator and a bending load cell with a range of 0 N − 120 N and an accuracy of ± 0.02 N. As a result, the minimum of the $|S_{11}(f)|$ curve of the combined system - planar resonator plus material under test was acquired, and it represents the system

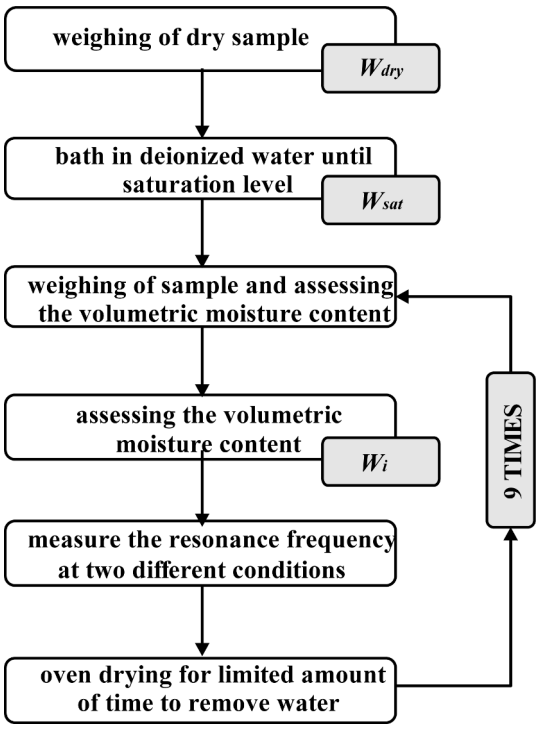

Fig. 5. Moistening procedure.

resonance frequency.

In the second step, the amount of absorbed water (θ_v) after immersion in deionized water was measured, modifying the UNI EN 13,755 [54]. Specimens were initially saturated by immersion in deionized water and then dried and weighed at regular time intervals. After each passage in the oven, we waited a short time to allow the water film over the surface to evaporate and for the cooling down of the sample, which may compromise the measurement process. In any case, the adopted measurement method is somehow sensitive to the "average" properties of the sample over the sensitive volume of the patch, which extends to a depth of about 1 cm. Therefore, the obtained results should not be particularly affected by a slight inhomogeneity in the internal moisture distribution. The moistening procedure is reported in Fig. 5.

In particular, W_{dry}, W_{sat}, and W_i represent the weight at dry, saturated, and i-th conditions. The percentage water content θ_v was given by

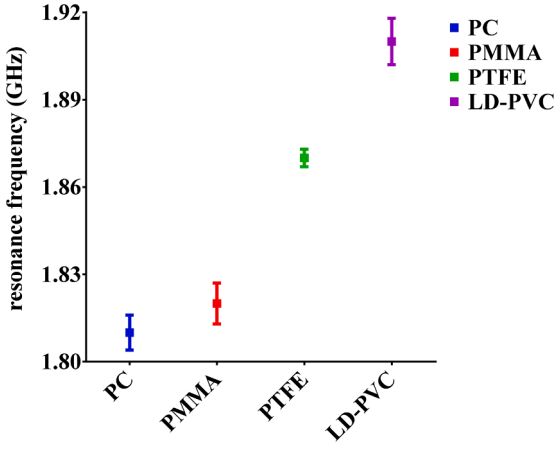

Fig. 6. Resonant frequency for known material with highlighted statistically significant differences among each material under test.

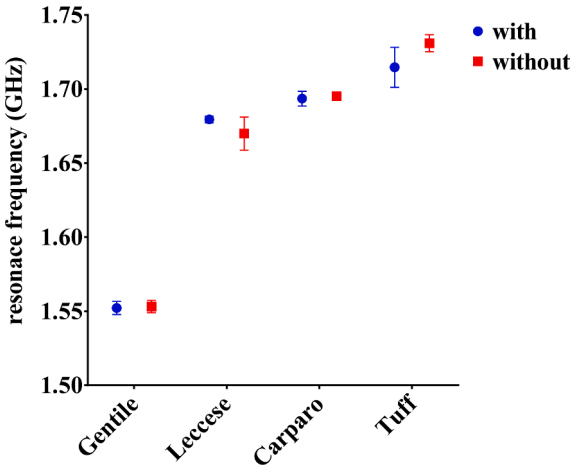

Fig. 7. Resonance frequency measured with and without aluminum foil on the back of the samples.

Eq. (1), and it was provided by the ratio between the difference of i-th weight and dried weight and the product of stone volume V and the density of water ρ

$$\theta_v = \frac{W_i - W_{dry}}{V \cdot \rho} \cdot 100, \quad (1)$$

for each of the eight tested moisture levels, we calculated the system repeatability expressed by the standard deviation (σ), by measuring ten times the reflection scattering in two different conditions:

- Uncontrolled applied force ("hand" case);
- Controlled applied force: $F = 20$ N ("load cell" case).

The first case exemplifies a manually applied force without an alert. In contrast, the second case represents the ideal application in which the technician uses a specific step that provides closed-loop control of the force applied over the brick. This setup is used to evaluate the calibration curve, useful for on-site applications. Nevertheless, the proposed method could acquire and evaluate "relative fluctuations" of moisture starting at a specific time, without previous calibration: a positive Δf_r means reducing humidity while a negative Δf_r represents an increasing water content. For each condition, ten repetitions were done, average value and an expanded uncertainty U equal to two times the standard deviation (***2σ***) were evalauted.

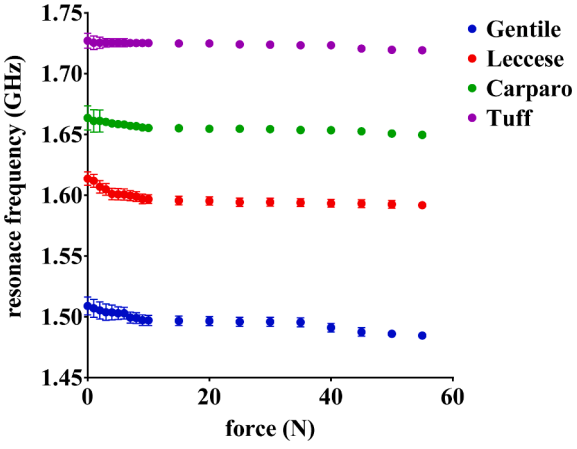

Fig. 8. Relationship between the applied force (0 N to 55 N range) and the resonance frequency.

Table 3
Gentile Stone. Comparison between the resonance frequency and the θ_v for the force applied with load cell and without control

Gentile Stone				
humidity	Load cell		Hand	
	f_r (GHz)	2σ (GHz)	f_r (GHz)	2σ (GHz)
0.0%	1.469	0.061	1.465	0.091
1.8%	1.371	0.053	1.370	0.075
3.6%	1.327	0.025	1.325	0.038
5.5%	1.295	0.036	1.288	0.083
7.3%	1.259	0.014	1.261	0.071
9.1%	1.227	0.029	1.228	0.098
10.9%	1.215	0.028	1.213	0.079
12.8%	1.192	0.043	1.196	0.080
14.6%	1.155	0.021	1.154	0.054

Table 4
Leccese Stone. Comparison between the resonance frequency and the θ_v for the force applied with load cell and without control

Leccese Stone				
humidity	Load cell		hand	
	f_r (GHz)	2σ (GHz)	f_r (GHz)	2σ (GHz)
0.0%	1.590	0.042	1.591	0.089
3.4%	1.532	0.015	1.547	0.025
8.3%	1.438	0.010	1.417	0.027
10.1%	1.360	0.024	1.373	0.032
13.5%	1.321	0.009	1.327	0.028
16.8%	1.217	0.022	1.211	0.061
20.2%	1.180	0.009	1.175	0.085
23.6%	1.127	0.039	1.128	0.073
26.9%	1.089	0.014	1.086	0.091

3. Results and discussion

3.1. Preliminary test results

Preliminary tests with well-known materials showed how the sensor is able to detect and identify materials with permittivity similar to the permittivity of the masonry unit under test, even if they are close to each other. Fig. 6 shows the frequency shift obtained testing the four plastic materials reported in the materials and methods section. One-way ANOVA reported significant differences in the resonant frequency among all the four plastic materials.

By the graduation curve presented and discussed in [52] we obtain the following values:

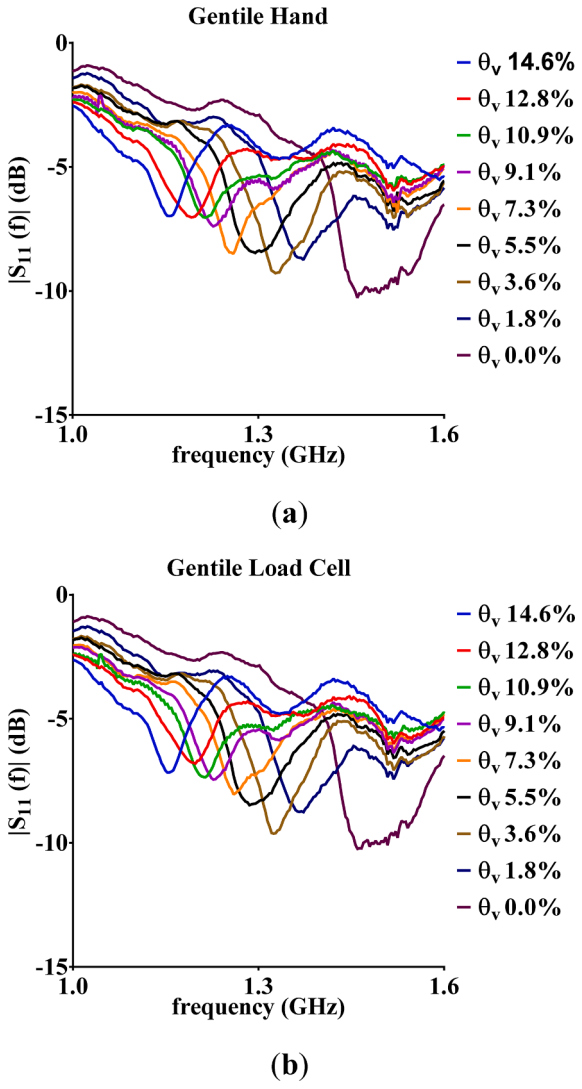

Fig. 9. The relation between the reflection coefficient and the θ_v for Gentile Stone. (**a**) Force applied with load cell, (**b**) Force applied without control.

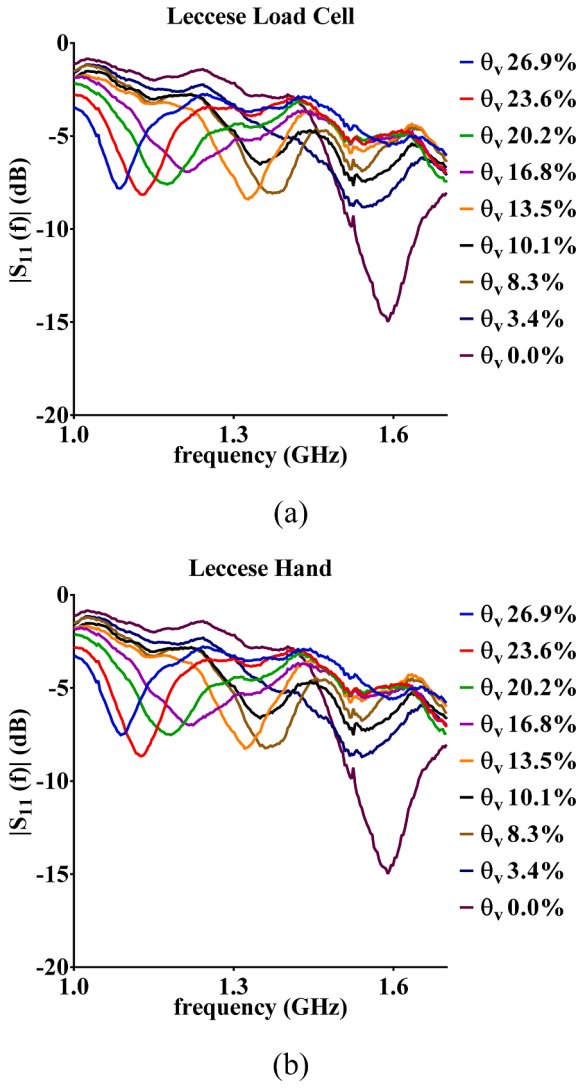

Fig. 10. The relation between the reflection coefficient and the θ_v for Leccese Stone. (**a**) Force applied with load cell, (**b**) Force applied without control.

Table 5
Carparo Stone. Comparison between the resonance frequency and the θ_v for the force applied with load cell and without control

Carparo Stone				
humidity	*Load cell*		*hand*	
	f_r (GHz)	2σ (GHz)	f_r (GHz)	2σ (GHz)
0.0%	1.628	0.007	1.683	0.010
3.3%	1.580	0.015	1.584	0.031
4.1%	1.542	0.023	1.545	0.074
8.3%	1.521	0.070	1.525	0.096
12.4%	1.344	0.067	1.334	0.098
16.5%	1.310	0.053	1.301	0.079
20.7%	1.230	0.039	1.227	0.098
24.8%	1.114	0.059	1.117	0.075
28.9%	1.101	0.047	1.111	0.095

Table 6
Tuff Stone. Comparison between the resonance frequency and the θ_v for the force applied with load cell and without control.

Tuff Stone				
humidity	*Load cell*		*hand*	
	f_r (GHz)	2σ (GHz)	f_r (GHz)	2σ (GHz)
0.0%	1.746	0.049	1.748	0.095
3.4%	1.532	0.041	1.518	0.081
6.9%	1.431	0.062	1.434	0.092
10.0%	1.334	0.071	1.327	0.082
13.3%	1.238	0.083	1.232	0.098
17.1%	1.181	0.075	1.176	0.095
20.5%	1.156	0.073	1.153	0.097
24.2%	1.149	0.088	1.149	0.098
27.8%	1.072	0.095	1.052	0.105

- we measured a value of $\varepsilon_r = 2.95 \pm 0.08$ for PC, against a value of 2.82 from the literature with an error of 5.2%;
- we measured a value of $\varepsilon_r = 2.74 \pm 0.18$ for PMMA, against a value of 2.60 from the literature with an error of 5.2%;
- we measured a value of $\varepsilon_r = 2.22 \pm 0.06$ for PTFE, against a value of 2.06 from the literature with an error of 5.5%;
- we measure a value of $\varepsilon_r = 1.68 \pm 0.09$ for LD-PVC against 1.62 from literature with an error of 5.8%.

Moreover, as reported in Fig. 7, no significant variations occurred when performing the measurements with an aluminum foil on the back of the sample. The 2-way ANOVA showed a p-value of 0.1548 for the

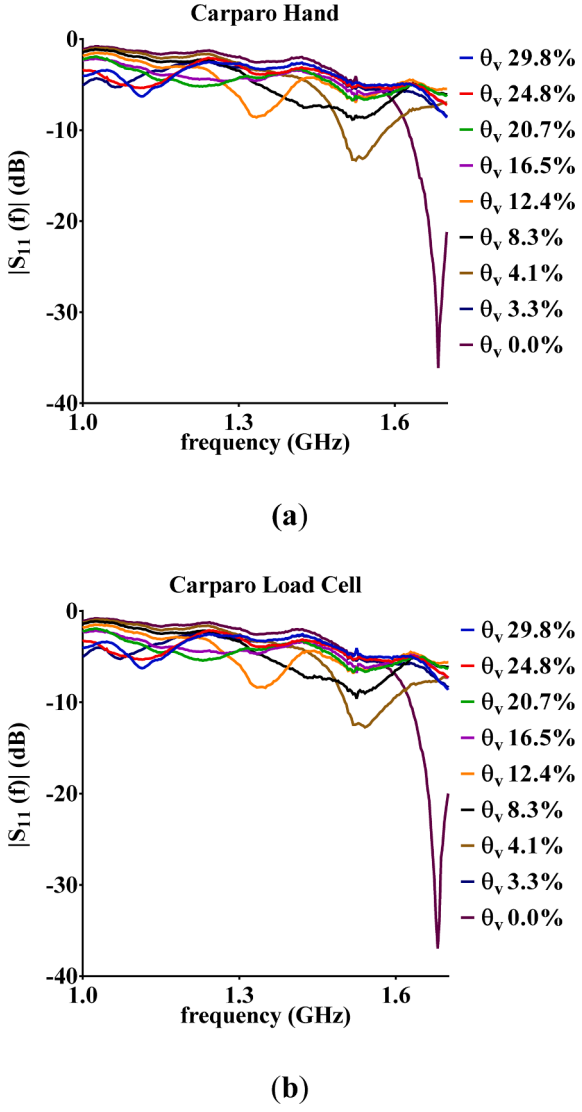

Fig. 11. The relation between the reflection coefficient and the θ_v for Carparo Stone. (**a**) Force applied with load cell, (**b**) Force applied without control.

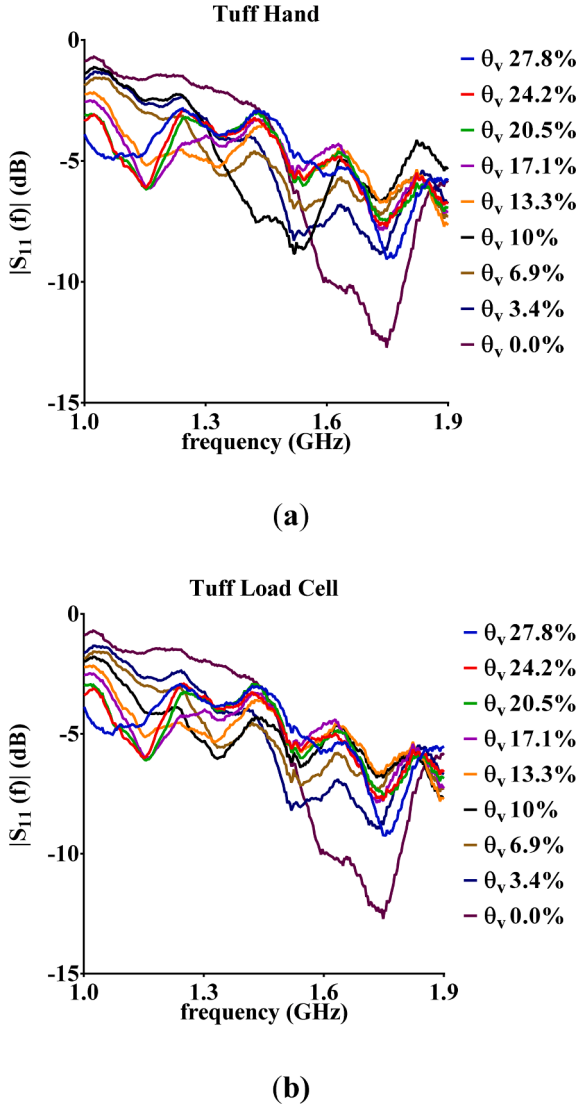

Fig. 12. The relation between the reflection coefficient and the θ_v for Tuff Stone. (**a**) Force applied with load cell, (**b**) Force applied without control.

fixed factor aluminum foil, while it showed a $p < 0.0001$ for the fixed factor stone type. A "post hoc" test analysis showed a statistically significant difference among the values of frequency measured for each pair of stones.

3.2. Force-resonance frequency results

Fig. 8 shows the relationship between the applied force and the resonance frequency for the four tested stones. In particular, the figure shows how an increment of the force produces a substantial frequency shift until a limit point beyond which the frequency variation was<10 MHz or stationary. This limit was measured to start at 15 N.

Another significant result concerns the increase in the repeatability of the measurements; the standard deviation was higher for low applied force than the standard deviation at high pressures. This result allowed more accurate measurements for rough surfaces where a greater adhesion was required (*Carparo* and *Tuff*).

3.3. Humidity-resonance frequency results

According to the results obtained in the first steps, we then compared, for each material, the results obtained at nine different moisture levels at the condition when the applied force was not monitored and when the applied force was imposed to (20 ± 1) N using the load cell.

Table 3 and Fig. 9 show the results for Gentile Stone. For each tested humidity condition, the repeatability of the measurements was higher for the "load cell" case (2σ always lower than 62 MHz) than the "hand" case (2σ always lower than 100 MHz). In particular, a repeatable force yielded an increase in the repeatability when the material under test was close to the saturation level. From Fig. 9, it is also possible to observe how an increase in water content produces a resonance frequency shift proportional to it.

Table 4 and Fig. 10 show the results for Leccese Stone. Also, for this stone, the measurement repeatability was lower for the "hand" case ($2\sigma < 91$ MHz) than for the "load cell" case (9 MHz $< 2\sigma <$ 50 MHz). It is also possible to see how a non-repeatable force at high moisture levels highly affects global repeatability. By Fig. 10, it is always likely to observe how the increase in moisture levels produces a resonance frequency shift.

Carparo Stone showed similar results to Gentile and Leccese Stones, with a repeatability of the measurements higher for the "load cell" case (2σ lower than 70 MHz, case $\theta_v = 8.30\%$). For the "hand" case, the standard deviations for the nine humidity levels were between two and three times higher than the counterpart value measured with the load

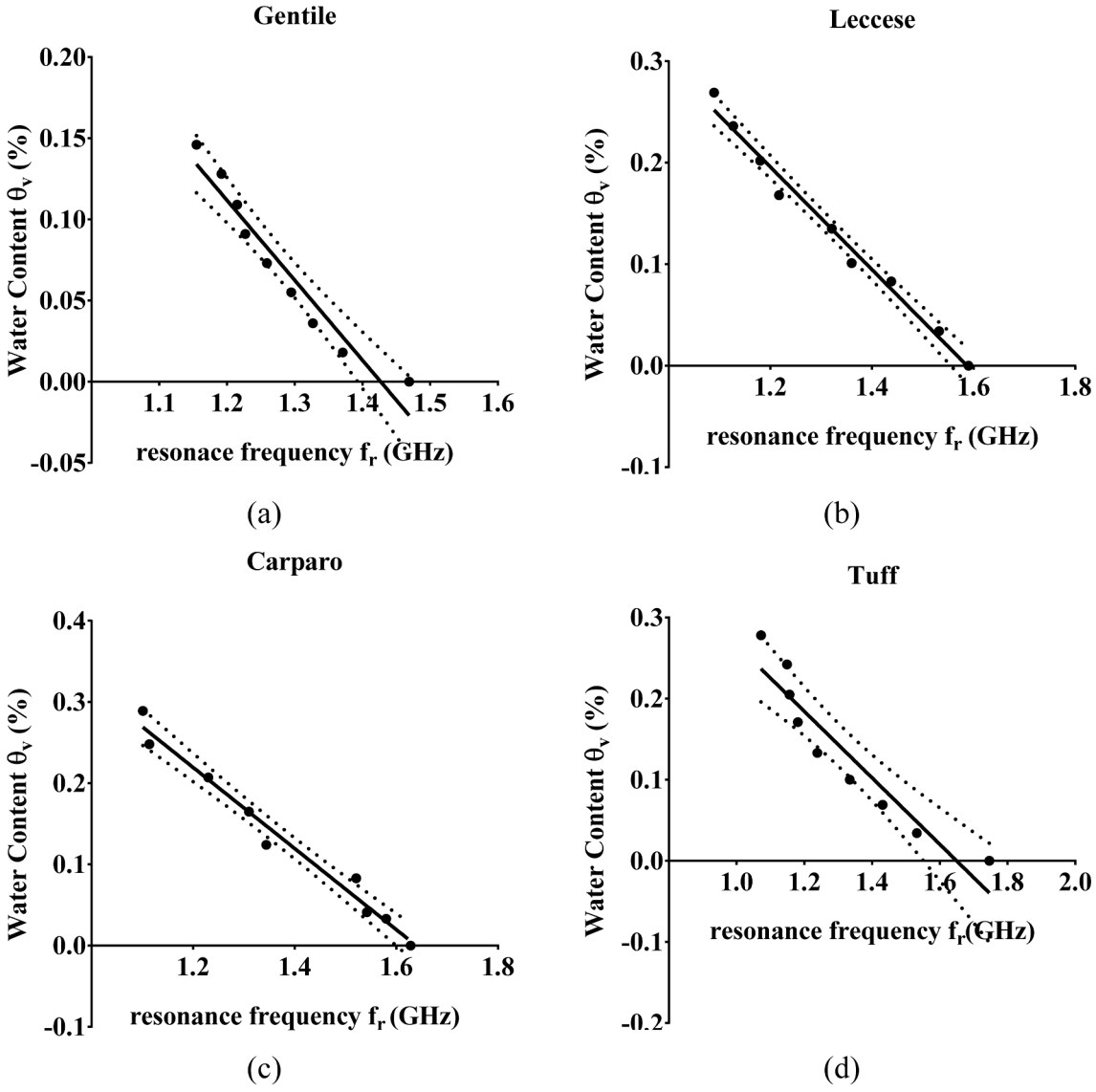

Fig. 13. Calibration curve with an external force equal to 20 N. (**a**) Gentile, (**b**) Leccese. (**c**) Carparo, (**d**) Tuff.

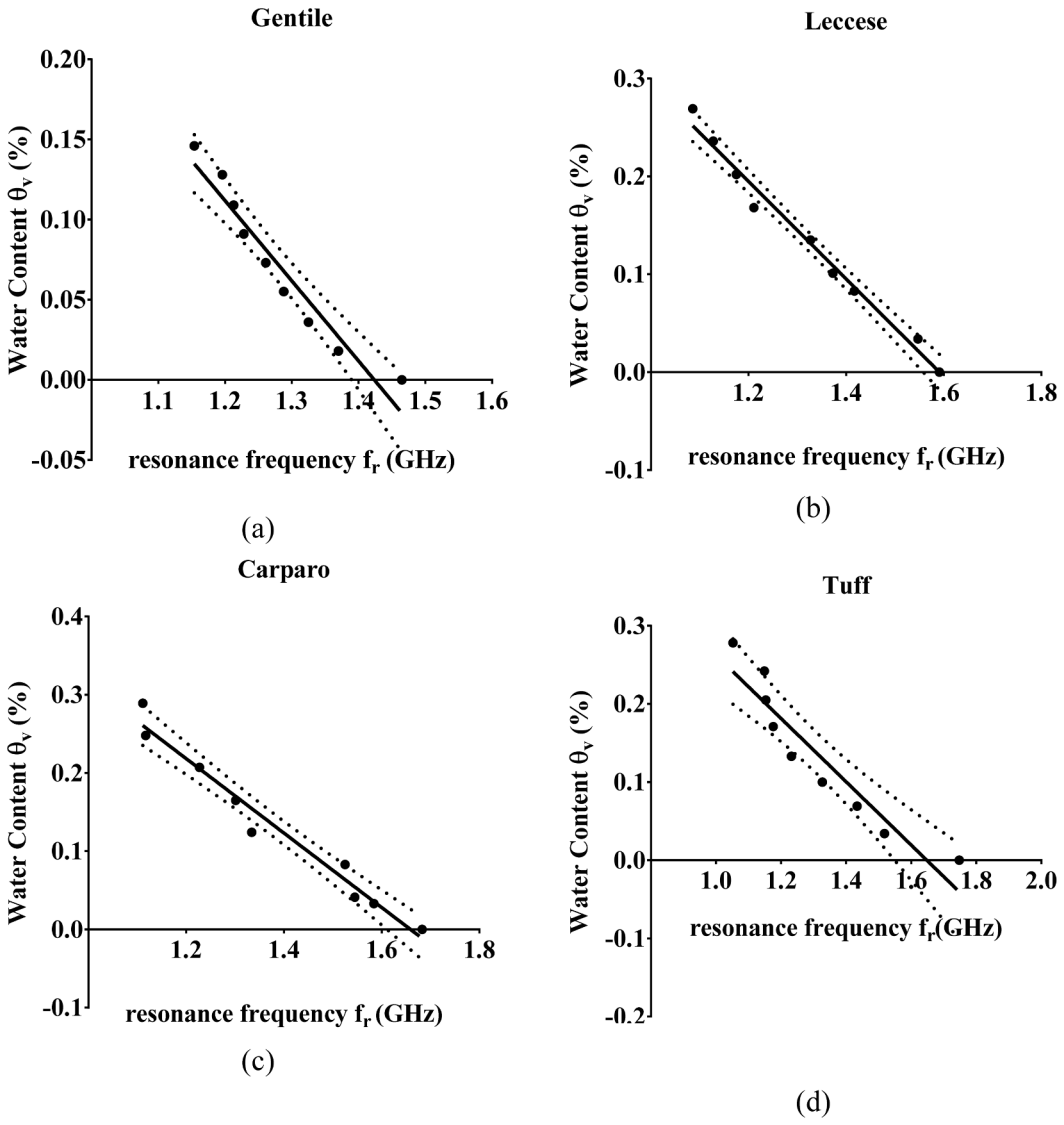

Fig. 14. Calibration curve with an unknown applied force. (**a**) Gentile, (**b**) Leccese. (**c**) Carparo, (**d**) Tuff.

Table 7
Calibration outline for "load cell" and "hand" condition.

Outline	Load Cell				Hand			
	Gentile	Leccese	Carparo	Tuff	Gentile	Leccese	Carparo	Tuff
R^2	0.94	0.99	0.98	0.89	0.93	0.98	0.97	0.89
RMSE	0.013	0.011	0.016	0.033	0.016	0.012	0.019	0.035
Fit-Dev_{max}	11.2%	5.2%	6.7%	12.6%	12.8%	6.0%	7.6%	12.8%

cell ($2\sigma < 0.098$ MHz). The discussed results are shown in Table 5 and Fig. 11, highlighting the relation frequency shift – moisture level.

Finally, the fourth material results are presented in Table 6 and Fig. 12. Despite the high anisotropy in terms of impurity and texture of the Tuff (Fig. 3d), the standard deviations were comparable with the Leccese species. Moreover, it is possible to observe the same attitude of the other materials regarding frequency shift (Fig. 12) and reduced repeatability corresponding to increased humidity (Table 6). Once again, results showed that non-repeatable force at high moisture levels affected global repeatability, and the use of a load cell to control the applied force increased the measurement repeatability.

Figs. 13 and 14 propose the graduation curves of $\theta_v - f_r$ useful for *non-invasive* on-site water content monitoring of Cultural Heritage structures. Fig. 13 shows the calibration curves when a load of 20 N was applied.

Gentile Stone presents a linear characteristic with a slope of −0.49, intercept of + 0.70, $R^2 = 0.94$, RMSE 0.013, and max deviation from the curve-fit (Fit-Dev_{max}) 11.2%; Leccese Stone presents a linear characteristic with a slope of −0.50, intercept of + 0.80, and $R^2 = 0.99$, RMSE 0.012 and Fit-Dev_{max} 5.5%; and Carparo Stone shows a linear characteristic with a slope of −0.50, intercept of + 0.82 and $R^2 = 0.98$, RMSE 0.016 and Fit-Dev_{max} 6.7%. Finally, Tuff gives a linear characteristic with a slope of −0.41, intercept of + 0.68, $R^2 = 0.89$, RMSE 0.033, and Fit-Dev_{max} 12.8%. This lower R^2 depends on a sudden change in slope over 15% of water content, similarly to moist powders grains, which present an exponential increase for high water content levels [55].

Table 8
Comparison between literature calibration values with highlighted the measurement conditions

Ref.	VNA	Load Condition	Best-fit values	Leccese	Carparo	Gentile
Piuzzi et al. [40]	Bench *Agilent E8363C*	not loaded	Slope	−0.48 ± 0.02	−0.47 ± 0.02	−0.42 ± 0.03
			Intercept	0.75 ± 0.03	0.80 ± 0.03	0.63 ± 0.04
			R^2	0.996	0.998	0.982
Present work	Portable *miniVNA*	Loaded at 20 N	Slope	−0.51 ± 0.02	−0.50 ± 0.03	−0.49 ± 0.05
			Intercept	0.80 ± 0.03	0.82 ± 0.04	0.70 ± 0.06
			R^2	0.985	0.978	0.937
		Unknown Load	Slope	−0.50 ± 0.03	−0,48 ± 0,03	−0.50 ± 0.05
			Intercept	0.79 ± 0.03	0,789 ± 0,05	0.71 ± 0.06
			R^2	0.984	0.969	0.935

Fig. 14 shows the calibration curves when an unknown load was applied. Gentile Stone presents a linear characteristic with a slope of −0.50, intercept of + 0.71, and $R^2 = 0.94$, RMSE 0.016 and Fit-Dev_{max} 12.8%; Leccese Stone presents a linear characteristic with a slope of −0.50, intercept of + 0.79, and $R^2 = 0.98$, RMSE 0.012 and Fit-Dev_{max} 6.0%; and Carparo Stone shows a linear characteristic with a slope of −0.48, intercept of + 0.79 and $R^2 = 0.97$, RMSE 0.019 and Fit-Dev_{max} 7.6%. Finally, Tuff gives a linear characteristic with a slope of −0.41, intercept of + 0.67, $R^2 = 0.89$, RMSE 0.035, and Fit-Dev_{max} 12.8%.

Table 7 summarizes the most significant outline of both calibration sets.

Moreover, Apulian stones present results compatible with our previous work [40], as shown in Table 8. In particular, it is also possible to observe that although the three Apulian stones present different linear equations, the uncertainty associated with each slope and intercept is compatible for all load conditions, showing the method robustness whether high-sensitivity (as in [40]) or low-cost equipment is used. Moreover, as discussed and presented in Tables 3–6, a controlled and steady external force reduces the measurement uncertainty and increases the determination coefficient R^2, making the proposed method suitable for on-site applications. Only Gentile stone presents an equation with a slope lower than literature values [40] and an R^2 lower than 0.98.

4. Conclusions

This paper presents a practical, portable, low-cost, easy-to-use reflectometric setup for moisture measurement in cultural heritage masonry units. The measurements were achieved for nine water content levels and four different materials, and the experimental relationship between each humidity level and the corresponding measured resonance frequency was derived. Experimental results showed that the calibration curves obtained with the miniVNA are well-matched with the results gained with bench instrumentations and show the method robustness and suitability with a maximum R^2 deviation of 4.79% for Gentile stone, 2.90% for Carparo, and 1.20% for Leccese stone. Furthermore, applying a steady external force, the measurement repeatability is increased with a standard deviation always lower than when the load is applied randomly.

As future developments, the sensor design improvement (geometries, two-port design for transmission measurements, loss tangent, fractional bandwidth and higher intrinsic Q-factor) and new materials (wood, modern, or painted brick) investigations will be carried on.

CRediT authorship contribution statement

Livio D'Alvia: Conceptualization, Writing – original draft, Writing – review & editing. **Erika Pittella:** Methodology, Data curation. **Emanuele Rizzuto:** Formal analysis. **Emanuele Piuzzi:** Supervision. **Zaccaria Del Prete:** Supervision.

Declaration of Competing Interest

The authors declare that they have no known competing financial interests or personal relationships that could have appeared to influence the work reported in this paper.

References

[1] M. Dautta, M. Alshetaiwi, J. Escobar, P. Tseng, Passive and wireless, implantable glucose sensing with phenylboronic acid hydrogel-interlayer RF resonators, Biosens. Bioelectron. 151 (2020) 112004, https://doi.org/10.1016/j.bios.2020.112004.

[2] S. Trabelsi, A.W. Krazsewski, S.O. Nelson, New density-independent calibration function for microwave sensing of moisture content in particulate materials, IEEE Trans. Instrum. Meas. 47 (3) (1998) 613–622, https://doi.org/10.1109/19.744310.

[3] E. Avşar Aydın and A. R. Torun, "3D printed PLA/copper bowtie antenna for biomedical imaging applications," *Phys. Eng. Sci. Med.*, vol. 43, no. 4, pp. 1183–1193, Dec. 2020, doi: 10.1007/s13246-020-00922-y.

[4] H. Amar, H. Ghodbane, M. Amir, M.A. Zidane, C. Hamouda, A. Rouane, Microstrip sensor for product quality monitoring, J. Comput. Electron. 19 (3) (Sep. 2020) 1329–1336, https://doi.org/10.1007/s10825-020-01517-2.

[5] M.P. Abegaonkar, R.N. Karekar, R.C. Aiyer, A microwave microstrip ring resonator as a moisture sensor for biomaterials: application to wheat grains, Meas. Sci. Technol. 10 (3) (Mar. 1999) 195–200, https://doi.org/10.1088/0957-0233/10/3/014.

[6] N.T.J. Ong, S.K. Yee, A.Y.I. Ashyap, Design of Microwave Sensor Based on Rectangular Double Split Ring Resonator for Water Quality Monitoring, in: 2020 IEEE Student Conference on Research and Development (SCOReD), 2020, pp. 111–116, https://doi.org/10.1109/SCOReD50371.2020.9250941.

[7] M.J. Varas-Muriel, E.M. Pérez-Monserrat, C. Vázquez-Calvo, R. Fort, Effect of conservation treatments on heritage stone. Characterisation of decay processes in a case study, Constr. Build. Mater. 95 (Oct. 2015) 611–622, https://doi.org/10.1016/j.conbuildmat.2015.07.087.

[8] E. Lucchi, L. Dias Pereira, M. Andreotti, R. Malaguti, D. Cennamo, M. Calzolari, V. Frighi, Development of a Compatible, Low Cost and High Accurate Conservation Remote Sensing Technology for the Hygrothermal Assessment of Historic Walls, Electronics 8 (6) (Jun. 2019) 643, https://doi.org/10.3390/electronics8060643.

[9] AA.VV, *The Effects of Air Pollution on Cultural Heritage*. Boston, MA: Springer US, 2009.

[10] D. Camuffo, Measuring Time of Wetness and Moisture in Materials, Microclim. Cult. Herit. (2019) 459–482, https://doi.org/10.1016/b978-0-444-64106-9.00019-5.

[11] F. Sandrolini, E. Franzoni, An operative protocol for reliable measurements of moisture in porous materials of ancient buildings, Build. Environ. 41 (10) (Oct. 2006) 1372–1380, https://doi.org/10.1016/j.buildenv.2005.05.023.

[12] F. Mangini, L. D'Alvia, M. Del Muto, L. Dinia, E. Federici, E. Palermo, Z. Del Prete, F. Frezza, Tag recognition: A new methodology for the structural monitoring of cultural heritage, Meas. J. Int. Meas. Confed. 127 (2018) 308–313, https://doi.org/10.1016/j.measurement.2018.06.003.

[13] P. Rotta, F. Abanto, W. Ipanaque, G. Ruiz, J. Soto, and J. Manrique, "A review of current methods for moisture content measurement," in *2019 IEEE CHILEAN Conference on Electrical, Electronics Engineering, Information and Communication Technologies (CHILECON)*, Nov. 2019, pp. 1–7, doi: 10.1109/CHILECON47746.2019.8987996.

[14] UNI EN 16682:2017, "Conservation of cultural heritage - Methods of measurement of moisture content, or water content, in materials constituting immovable cultural heritage." 2017.

[15] B. Blümich, F. Casanova, J. Perlo, F. Presciutti, C. Anselmi, B. Doherty, Noninvasive Testing of Art and Cultural Heritage by Mobile NMR †, Acc. Chem. Res. 43 (6) (Jun. 2010) 761–770, https://doi.org/10.1021/ar900277h.

[16] D. Capitani, V. Di Tullio, N. Proietti, Nuclear Magnetic Resonance to characterize and monitor Cultural Heritage, Prog. Nucl. Magn. Reson. Spectrosc. 64 (Jul. 2012) 29–69, https://doi.org/10.1016/j.pnmrs.2011.11.001.

[17] N. Proietti, D. Capitani, V. Di Tullio, Applications of Nuclear Magnetic Resonance Sensors to Cultural Heritage, Sensors 14 (4) (Apr. 2014) 6977–6997, https://doi.org/10.3390/s140406977.

[18] V. Di Tullio, N. Proietti, New Insights to Characterize Paint Varnishes and to Study Water in Paintings by Nuclear Magnetic Resonance Spectroscopy (NMR), Magnetochemistry 6 (2) (Apr. 2020) 21, https://doi.org/10.3390/magnetochemistry6020021.

[19] K.M. Aguilar-Castro, J.J. Flores-Prieto, E.V. Macías-Melo, Near infrared reflectance spectroscopy: Moisture content measurement for ceramic plaster, J. Mech. Sci. Technol. 28 (1) (Jan. 2014) 293–300, https://doi.org/10.1007/s12206-013-0964-3.

[20] G.M. Carlomagno, R. Di Maio, M. Fedi, C. Meola, Integration of infrared thermography and high-frequency electromagnetic methods in archaeological

surveys, J. Geophys. Eng. 8 (3) (Sep. 2011) S93–S105, https://doi.org/10.1088/1742-2132/8/3/S09.
[21] A. Kylili, P.A. Fokaides, P. Christou, S.A. Kalogirou, Infrared thermography (IRT) applications for building diagnostics: A review, Appl. Energy 134 (Dec. 2014) 531–549, https://doi.org/10.1016/j.apenergy.2014.08.005.
[22] E. Barreira, R.M.S.F. Almeida, M. Moreira, An infrared thermography passive approach to assess the effect of leakage points in buildings, Energy Build. 140 (Apr. 2017) 224–235, https://doi.org/10.1016/j.enbuild.2017.02.009.
[23] H. Güneyli, S. Karahan, A. Güneyli, N. Yapıcı, Water content and temperature effect on ultrasonic pulse velocity of concrete, Russ. J. Nondestruct. Test. 53 (2) (Feb. 2017) 159–166, https://doi.org/10.1134/S1061830917020024.
[24] U. Lencis, A. Udris, A. Korjakins, Moisture Effect on the Ultrasonic Pulse Velocity in Concrete Cured under Normal Conditions and at Elevated Temperature, Constr. Sci. 14 (Jan. 2013), https://doi.org/10.2478/cons-2013-0011.
[25] S. Goodhew, R. Griffiths, T. Woolley, An investigation of the moisture content in the walls of a straw-bale building, Build. Environ. 39 (12) (Dec. 2004) 1443–1451, https://doi.org/10.1016/j.buildenv.2004.04.003.
[26] C. Brischke, A.O. Rapp, R. Bayerbach, Measurement system for long-term recording of wood moisture content with internal conductively glued electrodes, Build. Environ. 43 (10) (Oct. 2008) 1566–1574, https://doi.org/10.1016/j.buildenv.2007.10.002.
[27] P. Palma, R. Steiger, Structural health monitoring of timber structures – Review of available methods and case studies, Constr. Build. Mater. 248 (2020) 118528, https://doi.org/10.1016/j.conbuildmat.2020.118528.
[28] P.K. Larsen, Determination of Water Content in Brick Masonry Walls using a Dielectric Probe, J. Archit. Conserv. 18 (1) (Jan. 2012) 47–62, https://doi.org/10.1080/13556207.2012.10785103.
[29] A. Aichholzer, C. Schuberth, H. Mayer, H. Arthaber, Microwave testing of moist and oven-dry wood to evaluate grain angle, density, moisture content and the dielectric constant of spruce from 8 GHz to 12 GHz, Eur. J. Wood Wood Prod. 76 (1) (Jan. 2018) 89–103, https://doi.org/10.1007/s00107-017-1203-x.
[30] D. Camuffo, C. Bertolin, P. Schenal, A novel proxy and the sea level rise in Venice, Italy, from 1350 to 2014, Clim. Change 143 (1–2) (Jul. 2017) 73–86, https://doi.org/10.1007/s10584-017-1991-3.
[31] S. Tanaka, K. Shiraga, Y. Ogawa, Y. Fujii, S. Okumura, Applicability of effective medium theory to wood density measurements using terahertz time-domain spectroscopy, J. Wood Sci. 60 (2) (Apr. 2014) 111–116, https://doi.org/10.1007/s10086-013-1386-7.
[32] C. Riminesi, E. Marie-Victoire, M. Bouichou, R. Olmi, Moisture and salt monitoring in concrete by evanescent field dielectrometry, Meas. Sci. Technol. 28 (1) (2017) 014002, https://doi.org/10.1088/1361-6501/28/1/014002.
[33] A. Szypłowska, M. Kafarski, A. Wilczek, A. Lewandowski, W. Skierucha, Salinity index determination of porous materials using open-ended probes, Meas. Sci. Technol. 28 (1) (2017) 014006, https://doi.org/10.1088/1361-6501/28/1/014006.
[34] F. Abe, A. Nishi, H. Saito, M. Asano, S. Watanabe, R. Kita, N. Shinyashiki, S. Yagihara, M. Fukuzaki, S. Sudo, Y. Suzuki, Dielectric study on hierarchical water structures restricted in cement and wood materials, Meas. Sci. Technol. 28 (4) (2017) 044008, https://doi.org/10.1088/1361-6501/aa5c65.
[35] J.S. Selker, L. Graff, T. Steenhuis, Noninvasive Time Domain Reflectometry Moisture Measurement Probe, Soil Sci. Soc. Am. J. 57 (4) (1993) 934–936, https://doi.org/10.2136/sssaj1993.03615995005700040009x.
[36] J. Majcher, M. Kafarski, A. Wilczek, A. Woszczyk, A. Szypłowska, A. Lewandowski, J. Szerement, W. Skierucha, Application of a Monopole Antenna Probe with an Optimized Flange Diameter for TDR Soil Moisture Measurement, Sensors 20 (8) (Apr. 2020) 2374, https://doi.org/10.3390/s20082374.
[37] A. Cataldo, E. De Benedetto, G. Cannazza, S. D'Amico, L. Farrugia, G. Mifsud, E. Dimech, C.V. Sammut, R. Persico, G. Leucci, L. De Giorgi, Dielectric permittivity diagnostics as a tool for cultural heritage preservation: Application on degradable globigerina limestone, Measurement 123 (2018) 270–274, https://doi.org/10.1016/j.measurement.2018.03.078.
[38] Z. Suchorab, D. Majerek, V. Kočí, R. Černý, Time Domain Reflectometry flat sensor for non-invasive monitoring of moisture changes in building materials, Measurement 165 (2020) 108091, https://doi.org/10.1016/j.measurement.2020.108091.
[39] B. Souffaché, P. Kessouri, P. Blanc, J. Thiesson, A. Tabbagh, First Investigations of In Situ Electrical Properties of Limestone Blocks of Ancient Monuments, Archaeometry 58 (5) (2016) 705–721, https://doi.org/10.1111/arcm.v58.510.1111/arcm.12204.
[40] E. Piuzzi, E. Pittella, S. Pisa, A. Cataldo, E. De Benedetto, G. Cannazza, An improved noninvasive resonance method for water content characterization of Cultural Heritage stone materials, Measurement 125 (Sep. 2018) 257–261, https://doi.org/10.1016/j.measurement.2018.04.070.
[41] L. D'Alvia, E. Piuzzi, E. Pittella, and Z. Del Prete, "Effect of Applied Pressure on Patch Resonator- Based Measurements of Moisture Level for Cultural Heritage Materials," *IEEE Int. Conf. Metrol. Archaeol. Cult. Heritage, Cassino, Italy, Oct. 22-24*, pp. 20–22, 2018.
[42] L. D'Alvia, E. Palermo, Z. Del Prete, E. Pittella, S. Pisa, E. Piuzzi, "A comparative evaluation of patch resonators layouts for moisture measurement in historic masonry units", *2019 IMEKO TC4 Int*, Conf. Metrol. Archaeol. Cult. Heritage, MetroArchaeo 2019 (2019) 149–153.
[43] R. B. Waterhouse, *Microstrip Patch Antennas: A Designer's Guide*, vol. 7, no. 2. Boston, MA: Springer US, 2003.
[44] "Hardware Manual for miniVNA Tiny." pp. 1–2, 2014, [Online]. Available: https://www.wimo.com/media/manuals/MRS/MiniVNA_Tiny_Antennenanalysator_Antenna-Analyzer_Hardware-Manual_EN.pdf.
[45] S.V. Gupta, Mass Metrology, Strain Gauge Load Cells (2012) 89–119.
[46] AVIA SEMICONDUCTOR, "HX711 - Datasheet." [Online]. Available: https://www.mouser.com/datasheet/2/813/hx711_english-1022875.pdf.
[47] A. Colella, C. Di Benedetto, D. Calcaterra, P. Cappelletti, M. D'Amore, D. Di Martire, S.F. Graziano, L. Papa, M. de Gennaro, A. Langella, The Neapolitan Yellow Tuff: An outstanding example of heterogeneity, Constr. Build. Mater. 136 (2017) 361–373, https://doi.org/10.1016/j.conbuildmat.2017.01.053.
[48] A. Calia, M. Sileo, L. Matera, Provenance, characterization and decay of a porous calcarenite of the Puglia region ('Pietra Gentile'), Geol. Soc. London, Spec. Publ. 391 (1) (2014) 47–70, https://doi.org/10.1144/SP391.11.
[49] A. Calia, M. Laurenzi Tabasso, A. Maria Mecchi, G. Quarta, The study of stone for conservation purposes: Lecce stone (southern Italy), Geol. Soc. London, Spec. Publ. 391 (1) (2014) 139–156, https://doi.org/10.1144/SP391.8.
[50] N. Bianco, A. Calia, G. Denotarpietro, P. Negro, Laboratory Assessment of the Performance of New Hydraulic Mortars for Restoration, Procedia Chem. 8 (2013) 20–27, https://doi.org/10.1016/j.proche.2013.03.004.
[51] E. Piuzzi, G. Cannazza, A. Cataldo, S. Chicarella, E. De Benedetto, F. Frezza, S. Pisa, S. Prontera, F. Timpani, Measurement System for Evaluating Dielectric Permittivity of Granular Materials in the 1.7–2.6-GHz Band, IEEE Trans. Instrum. Meas. 65 (5) (2016) 1051–1059, https://doi.org/10.1109/TIM.2015.2495720.
[52] E. Piuzzi, G. Cannazza, A. Cataldo, E. De Benedetto, L. De Giorgi, F. Frezza, G. Leucci, S. Pisa, E. Pittella, S. Prontera, F. Timpani, A comparative assessment of microwave-based methods for moisture content characterization in stone materials, Measurement 114 (2018) 493–500, https://doi.org/10.1016/j.measurement.2016.04.046.
[53] K. Venu Madhava Rao, B. V. Venkatarama Reddy, and K. S. Jagadish, "Strength characteristics of stone masonry," *Mater. Struct.*, vol. 30, no. 4, pp. 233–237, May 1997, doi: 10.1007/BF02486181.
[54] UNI EN 13755, "Natural Stone Test Methods. Determination of Water Absorption at Atmospheric Pressure.".
[55] J. Peters, W. Taute, K. Bartscher, C. Döscher, M. Höft, R. Knöchel, J. Breitkreutz, Design, development and method validation of a novel multi-resonance microwave sensor for moisture measurement, Anal. Chim. Acta 961 (2017) 119–127, https://doi.org/10.1016/j.aca.2017.01.021.